Journal of the European Ceramic Society 22 (2002) 1683–1691

www.elsevier.com/locate/jeurceramsoc

Behavior of strontium titanate ceramics in reducing conditions suggesting enhanced conductivity along grain contacts

João C.C. Abrantes[a], João A. Labrincha[b], Jorge R. Frade[b,*]

[a]*ESTG, Instituto Politécnico de Viana do Castelo, Ap. 574, 4900 Viana do Castelo, Portugal*
[b]*Ceramics and Glass Engineering Dep. (UIMC), University of Aveiro, 3810 Aveiro, Portugal*

Received 7 March 2001; received in revised form 17 August 2001; accepted 19 September 2001

Abstract

In reducing conditions the resistance of dense strontium titanate ceramic samples decreases markedly with decreasing average grain size. This trend is interpreted on assuming enhanced conductivity along grain contacts in parallel with a RC bulk term. The temperature dependence is consistent with this model and indicates that the bulk may still control the overall behavior at sufficiently high temperatures (typically for $T>700$ °C). The resistivity of fine grained porous samples is intermediate between the results obtained for fine grained dense samples and dense samples with large average grain size. An extended model is thus proposed to describe the behavior of porous samples by assuming a series association of isolated channels connected by the interior of adjacent grains.

Keywords: Electrical conductivity; Grain boundaries; $SrTiO_3$

1. Introduction

The differences between the bulk and grain boundary properties are the basis for several types of applications of titanate ceramics. For example, strontium titanate ceramics can be used as grain boundary barrier layer capacitors (GBBLC).[1,2] These materials are heat treated in reducing conditions, and re-oxidized to obtain semiconducting grain interiors surrounded by very resistive grain boundaries. It is, thus, useful to understand the bulk and grain boundary transport properties in reducing conditions as well as in oxidizing conditions. In addition, the overall behavior is very dependent on the actual microstructural features such as the average grain size, which may be controlled by suitable additives, and/or changes in the Ti:Sr ratio.[3–5]

The GBBLC materials are usually doped with a suitable donor (e.g. Nb) to enhance the transport properties and to attain suitable microstructures.[5] Unfortunately the transport properties of donor doped titanates are difficult to study, except at very high temperatures ($T>1000$ °C),[6] and/or for porous samples.[7] These difficulties are probably related to the extremely slow kinetics of re-oxidation.

The conductivity of undoped and acceptor doped strontium titanate varies in similar ways on changing the working conditions (e.g. temperature and oxygen partial pressure).[8] The conductivity of these materials is mainly p-type in oxidizing conditions, and the overall behavior is often controlled by resistive grain boundaries.[9–11] Vollmann and coauthors[10] simulated the grain boundary conductivity profiles on assuming segregation of donor impurities at grain boundaries. In this case, space charge effects should depress the concentration profiles of positive charge carriers, thus yielding very resistive boundaries in oxidising conditions.

Impedance spectroscopy is often used to separate the contributions of the bulk, grain boundaries, and material/electrode interfaces, on assuming a brick layer model with series association of the bulk, resistive grain boundaries, and external material/electrode interfaces.[12] The applicability of the brick layer model was predicted by finite element studies, except possibly for somewhat unusual microstructures,[13] and was also demonstrated by plotting grain boundary resistance results (R_{gb}) for samples with different average grain sizes (d_g) as:[14]

* Corresponding author. Tel.: +351-234-370354; fax: +351-234-425300.
E-mail address: jfrade@cv.ua.pt (J.R. Frade).

0955-2219/02/$ - see front matter
PII: S0955-2219(01)00466-6

$$R_{gb}d_g(A/L) = \rho_{gb}\delta_{gb}, \quad (1)$$

where A is the electrode area, L is the samples thickness, ρ_{gb} is the grain boundary resistivity, and δ_{gb} is the thickness of a single grain boundary. One obtained a single trend for samples with different average grain sizes, as expected for the brick layer model. Similarly, the differences in grain boundary capacitance were accounted for by plotting:[14]

$$C_{gb}(L/A)d_g^{-1} = \varepsilon_o\varepsilon_r\delta_{gb}^{-1} \quad (2)$$

Under reducing conditions the bulk conductivity of strontium titanate based materials is mainly n-type, at least at sufficiently high temperatures.[8] Vollman et al.[10,15] also predicted a major change in grain boundary behaviour under reducing conditions with enhanced n-type charge transport along grain boundaries. This hypothesis may explain differences in electrical properties of $SrTiO_3$ thick films with different microstructures, in reducing conditions.[16] The present results obtained for strontium titanate ceramics in reducing conditions suggest enhanced charge transport along multiple grain contacts.

Fig. 1A shows a schematic representation (cross section) of a simple brick layer model for enhanced transport along grain boundaries. On assuming that the fast conducting channels correspond to interfaces between adjacent grains one obtains the area fraction of channels $(2\delta_{gb}d_g)/d_g^2 = 2\delta_{gb}/d_g$, and the corresponding resistance along grain boundaries:

$$R_{agb} = 0.5\rho_{gb}(L/A)\left(d_g/\delta_{gb}\right) \quad (3)$$

Eq. (3) predicts an increase in resistance along grain boundary with increasing grain size, and this may be rewritten to obtain one unique trend for samples with different grain sizes:

$$R_{agb}(A/L)d_g^{-1} = 0.5\rho_{gb}\delta_{gb}^{-1} \quad (4)$$

Enhanced charge transport along multiple grain contacts (Fig. 1B) may yield a stronger dependence on grain size. The sectional area fraction of such channels is $\left(\phi_{mc}/d_g\right)^2/g_f$, ϕ_{mc} being the equivalent diameter of multiple contacts and g_f a geometric factor. The resistance along multiple contact boundaries is then $R_{agb} = (L/A)\rho_{gb}g_f\left(d_g/\delta_{gb}\right)^2$, which yields:

$$R_{agb}(A/L)d_g^{-2} = g_f\rho_{gb}\delta_{gb}^{-2} \quad (5)$$

2. Experimental methods

Strontium titanate powders were prepared by calcination of mixtures of titania and strontium carbonate at 1100 °C, for 15 h. X-ray diffraction showed that these powders were single phase within the detection limit of the equipment. The calcined powders were milled to destroy agglomerates and used to prepare uniaxially pressed pellets. Different pellets were sintered in air and with the firing conditions shown in Table 1. The notations ST1600, ST1480, ST1400, and ST1300 indicate the firing temperatures 1600, 1480, 1400 and 1300 °C. Scanning electron microstructures (Fig. 2) were used to estimate the average grain size of samples ST1400 (A), ST1480 (B), ST1600 (C) and ST1300 (D). The density

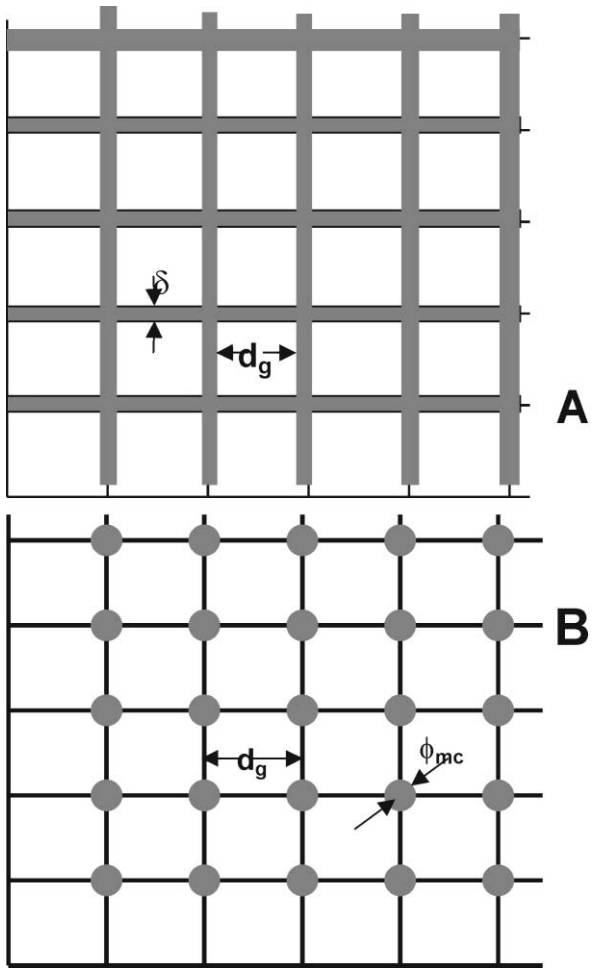

Fig. 1. Schematic representations of the cross sections of grain boundaries (A) or other multiple grain contacts (B) which might act as channels for enhanced charge transport.

Table 1
Sintering conditions and the corresponding average grain size and relative density values

Sample	Temperature (°C)	Time (h)	Grain size (μm)	Relative density
A	1600	20	≈31	≈99%
B	1480	20	≈11	≈99%
C	1400	4	≈3	≈98%
D	1300	4	<1	≈83%

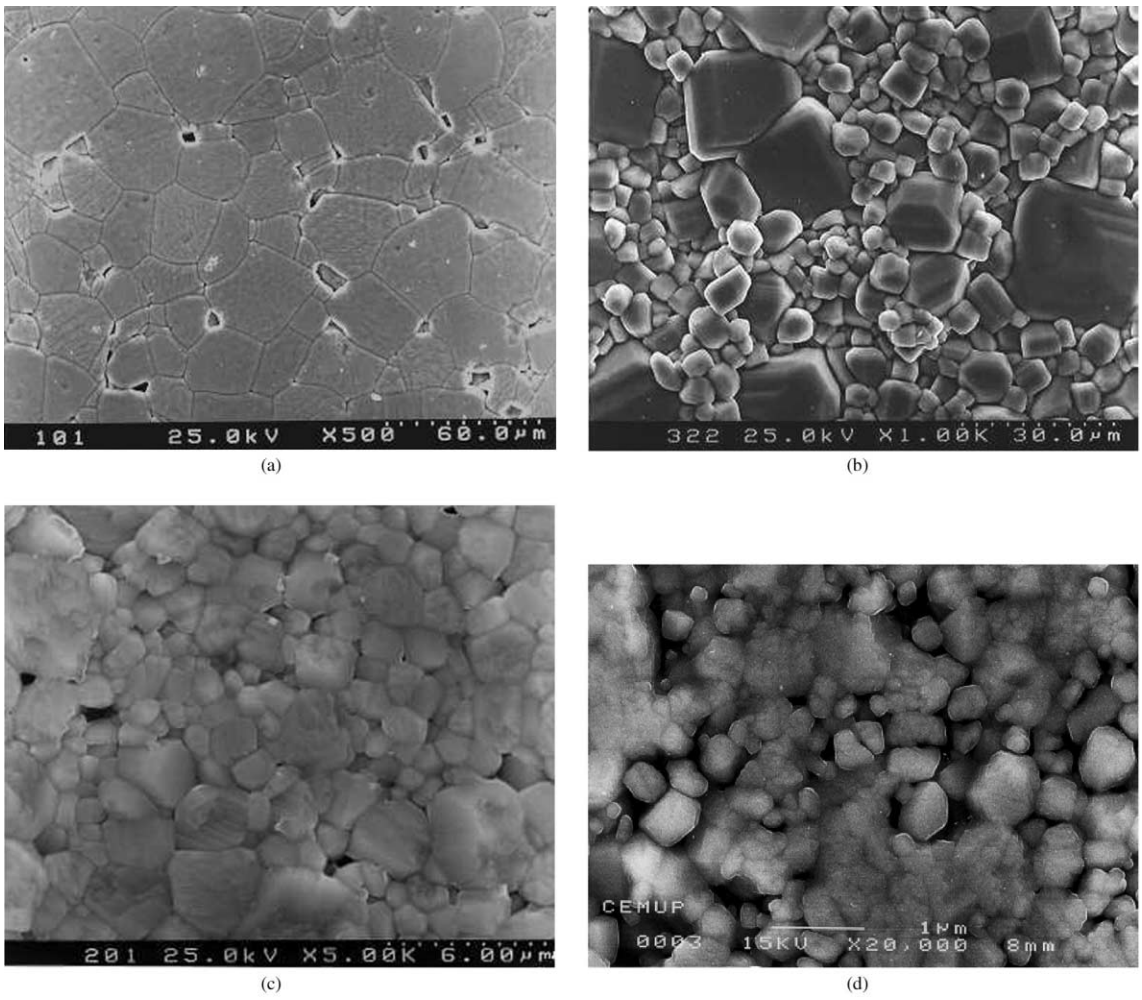

Fig. 2. Scanning electron microstructures of samples ST1400 (A), ST1480 (B), ST1600 (C) and ST1300 (D).

was measured by immersion in Hg, and the lattice parameter was used to evaluate the unit cell volume and the theoretical density. The density, and the average grain size increase with the firing temperature.

The HP428A precision LCR meter was used to obtain impedance spectra in the frequency range 20 Hz–1 MHz. The samples were disk-shaped with a diameter of about 10 mm, and thickness of about 2 mm. Porous Pt electrodes were painted onto the surfaces of these samples, and fired at 1000 °C. The measurements were performed at temperatures in the range 300–1000°C, and with different atmospheres, in a furnace equipped with a potentiometric oxygen sensor to monitor the oxygen partial pressure. Every sample was equilibrated at 1000 °C in a reducing gas mixture (95% N_2 + 5% H_2), for about 2 h, before the electrical measurements. This gas mixture was kept flowing at 100–200 ml/min while the measurements were performed with average cooling rates in the range of −1 to −2 °C/min.

The actual values of oxygen partial pressure are somewhat dependent on the cooling rate, and on the flow of the 95% N_2 + 5% H_2 gas mixture, as shown in Fig. 3; this indicates that one must control the cooling rate and the flux to be able to compare the results obtained for different samples. However, the furnace inertia may limit the effective cooling rate at relatively low temperatures. For example, the cooling rate cannot exceed −2 °C/min at 600 °C, or −1 °C/min at 300 °C. The open symbols in Fig. 3 thus represent spontaneous cooling of the furnace, rather than at the programmed cooling rate. The change in Po_2 can be accounted for by taking into account the Gibbs free energy and mass action law of $2H_2 + O_2 \Longleftrightarrow 2H_2O$; this yields $P_{O_2} = (pH_2O/pH_2).\exp(\Delta G/RT)$, for a nearly constant water vapour to hydrogen ratio in the atmosphere, or $-\log(P_{O_2}) = 20.6$, 21.4, 27.0, and 35.7 at 1000, 800, 600 and 400 °C respectively for $pH_2O/pH_2 = 0.03$. These predictions are close to the results in Fig. 3.

The conductivity of strontium titanate is n-type in very reducing conditions, and one may thus use the following dependence[8]

$$\sigma_n = \sigma_{n,1}\left(P_{O_{2,ref}}/P_{O_2}\right)^{1/6} \quad (6)$$

where $\sigma_{n,1}$ denotes the conductivity at the reference value of oxygen partial pressure ($P_{O_{2,ref}} = 1$ atm). Eq. (6) may then be rewritten as:

$$\sigma_{n,1} = (L/A)(P_{O_2}/P_{O_{2,ref}})^{1/6}.R^{-1} \quad (7)$$

to compensate for differences in oxygen partial pressure related to changes in working conditions (cooling rate, flow rate, etc), as demonstrated in Fig. 4. In this case, the working conditions only affect these results at relatively low temperatures, probably because the reliability of the oxygen sensor tends to decrease with decreasing temperatures.

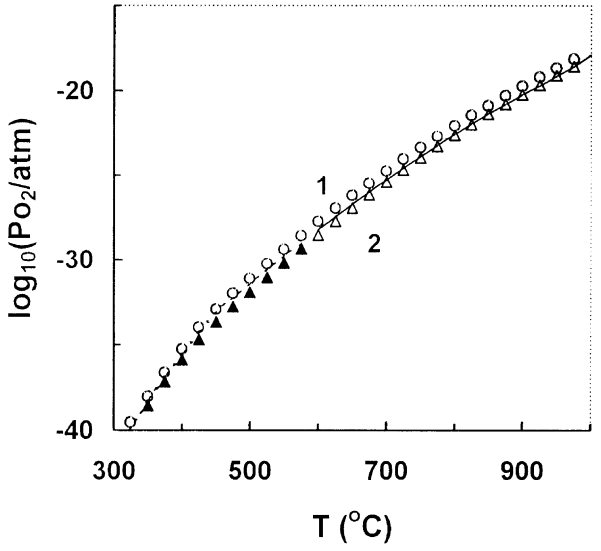

Fig. 3. Temperature dependence of the oxygen partial pressure in the furnace used for the electrical measurements, and for: (i) cooling rate −1 °C/min and gas flow rate 200 ml/min (circles); (ii) −2 °C/min and 200 ml/min (triangles); (iii) −2 °C/min and 100 ml/min (solid line).

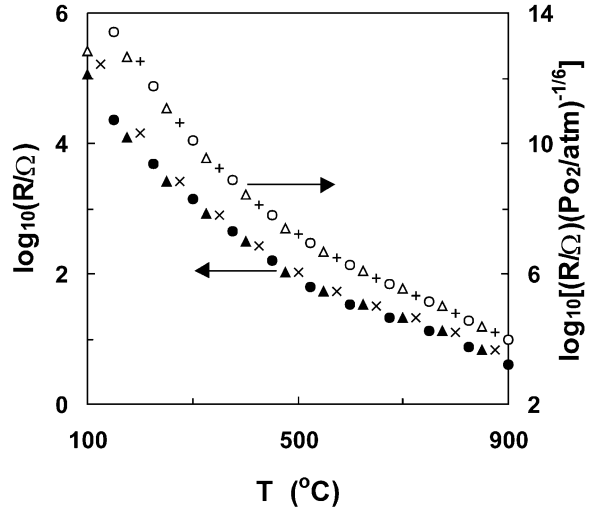

Fig. 4. Temperature dependence of resistance of sample ST1400 (closed symbols and ×), and the corresponding compensation for differences in oxygen partial pressure (open symbols and +), for: (i) cooling rate −1 °C/min and gas flow rate 200 ml/min (circles); (ii) −2 °C/min and 200 ml/min (triangles); (iii) −2 °C/min and 100 ml/min (x, +).

3. Results

Fig. 5A–D show normalized impedance spectra obtained for samples ST1600, ST1480, ST1400 and ST1300 cooled from 1000 °C in 95% N_2 + 5% H_2. The behavior of dense samples (ST1600 and ST1480) is nearly described by a simple *RC* term, and a small contribution in the low frequency range can be ascribed to the external material/electrode interface.

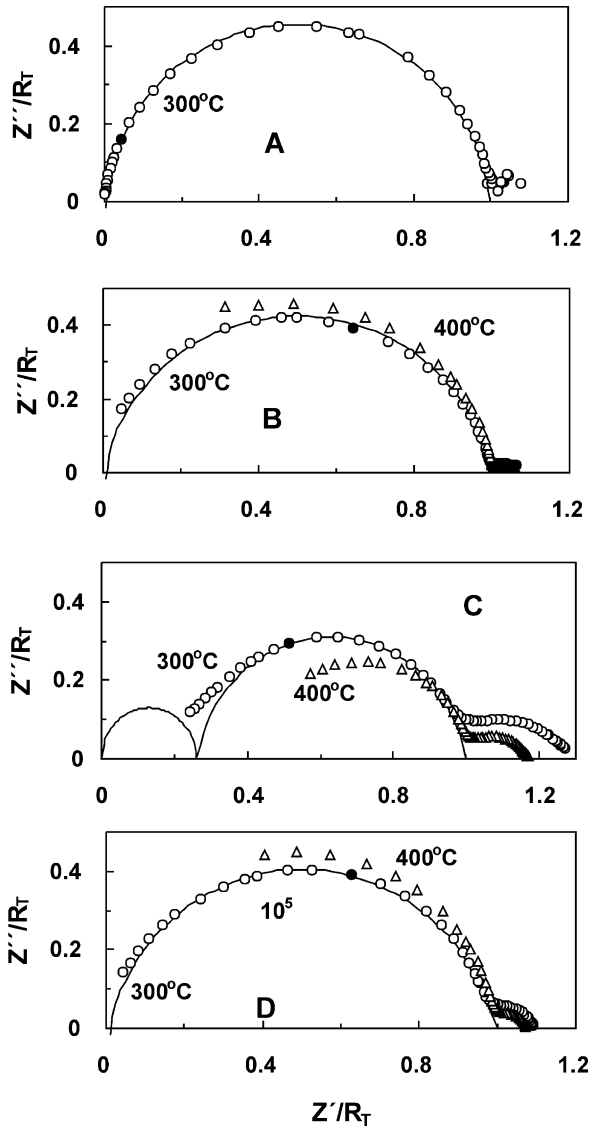

Fig. 5. Normalized impedance spectra obtained for samples ST1600 (A), ST1480 (B), ST1400 (C), and ST1300 (D) cooled in 95% N_2 + 5% H_2, and measured at 300 °C (○), 400 °C (△), 500 °C (+), 600 °C (X). The values of resistivity RA/L of samples ST1600, ST1480, ST1400 and ST1300 are 1.43×10^3, 125, 12.1, and 165 Ω.cm respectively at 300 °C, and 270, 35.1, 2.30, and 29.8 Ω.cm respectively at 400 °C.

The actual Nyquist plots show somewhat depleted arcs rather than perfect semicircles. These deviations are commonly found for most materials,[13,17] and may be accounted for by assuming a constant phase angle element (CPE) component rather than a capacitance, as described by:

$$Z* = R/[1 + (i\omega C)^{1-\alpha}R] + R_{el}/[1 + (i\omega C_{el})^{1-\beta}R], \quad (8)$$

with $0 < \alpha << 1$, and $0 < \beta < 1$. Suitable codes developed by Boukamp[17] were used to obtain the values of resistance (Fig. 6), and pseudocapacitance. The high temperature behavior is typically n-type in very reducing conditions, and it is thus convenient to compare results for the reference oxygen partial pressure (Fig. 6) to compensate for eventual changes of oxygen partial pressure in the 95% N_2 + 5% H_2 gas mixture.

The values of pseudocapacitance may differ from the true capacitance, and this was thus evaluated as a function of peak frequency f_{peak} and resistance as follows:

$$C = 1/(2\pi f_{peak} R) \quad (9)$$

These values were then used to obtain the dielectric constant shown in Fig. 7, $C(L/A)/\varepsilon_o$ where ε_o is the permitivity of vacuum.

These values of capacitance and the corresponding values of $C(L/A)/\varepsilon_o$ are about twice the corresponding results reported for strontium titanate single crystals[9] and for strontium titanate ceramics in air[14] ($\varepsilon_r \approx 300$). Nevertheless, the actual results are still within the range of results obtained for strontium titanate ceramics in an atmosphere of N_2 (Abrantes et al.[14]). It thus seems that the measured values of capacitance represent a bulk term rather than a grain boundary capacitance, which is usually at least one order of magnitude higher.[11,14] The capacitance of the additional contribution of electrode/sample interfaces is usually even higher than for the grain boundary term.[11]

4. Enhanced transport along grain contacts

On comparing the results for samples ST1600 and ST1400 (Fig. 6) one concludes that an increase of one order of magnitude in average grain size causes an increase in the low temperature resistance by about 2 orders of magnitude. This effects thus suggests the dependence predicted for enhanced charge transport along multiple grain contacts, as predicted by Eq. (5), and shown in Fig. 8.

The equivalent circuit shown in Fig. 9 is an attempt to describe the parallel contributions of charge transport in the bulk and enhanced transport along grain boundaries or along other types of multiple grain contacts. In this case, the measured capacitance still corresponds to the bulk capacitance:

$$C \approx C_B, \quad (10)$$

and a parallel association of the bulk resistance R_B and the resistance to charge transport along generic grain contacts R_{agc} becomes:

$$R = (1/R_B + 1/R_{agc})^{-1} \quad (11)$$

Enhanced conductivity along grain contacts may thus explain the decrease in resistance with decreasing grain size, as found on comparing the results obtained for

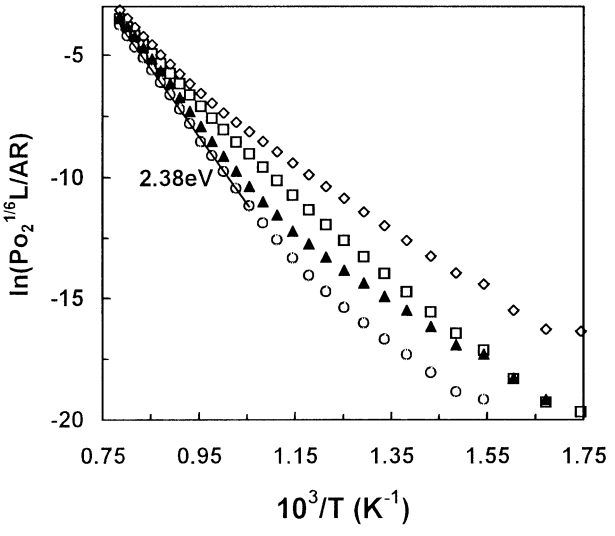

Fig. 6. Conductivity results obtained for samples ST1600 (○), ST1480 (▲), ST1300 (□), and ST1400 (◇) after correction for differences in the electrode area to thickness ratio (A/L), and/or oxygen partial pressure.

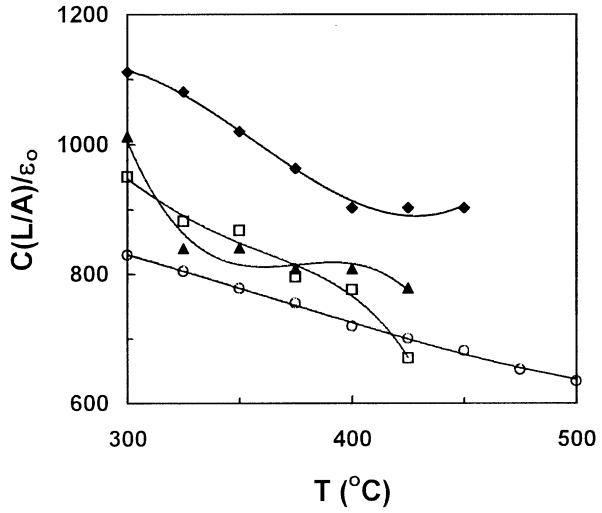

Fig. 7. Capacity values obtained for samples ST1600 (○), ST1480 (▲), ST1300 (□), and ST1400 (◆) after correction for differences in the thickness to electrode area ratio (L/A).

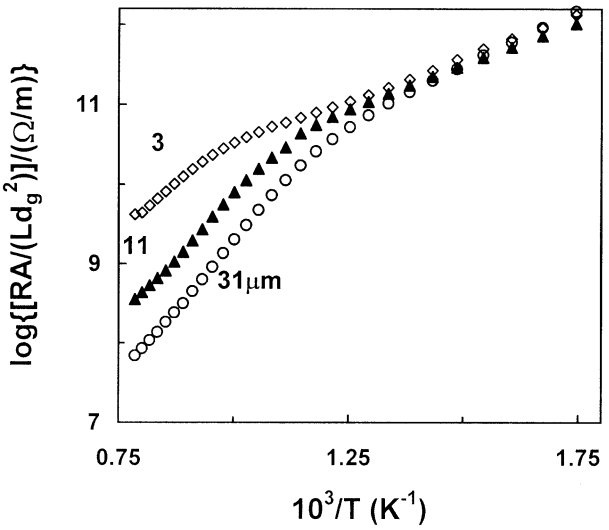

Fig. 8. Alternative representation of resistivity data obtained for samples ST1600 (○), ST1480 (▲), and ST1400 (◆) as predicted for enhanced charge transport along multiple grain contacts.

samples ST1600, ST1480, and ST1400, with typical average grain sizes of about 32, 11 and 3 μm respectively. However, the overall trend is reverted on comparing the results obtained for sample ST1400 (with a typical average grain size of about 3 μm), and a porous sample (ST1300) with grain size smaller than 1 μm (Fig. 6). In this case, the differences can be explained by taking into account that porosity (or other types of discontinuities) may hinder the enhanced transport along grain contacts, as illustrated in Fig. 10A. A somewhat different equivalent circuit is thus proposed for this case (Fig. 10B). The bridging elements with resistance R_{br} and capacitance C_{br} correspond to connections through nearby grain interiors.

R_{br} is expected to increase with porosity, and may become much greater than the resistance along grain boundaries, ($R_{br} >> R_{agb}$), at least for very porous samples (e.g. ST1300). Nevertheless, the resistance of the bridging element may still correspond to a small fraction of the total resistance of grain interiors ($R_{agb} << R_{br} << R_B$). In this case the overall behavior of porous samples may still be nearly described by a simple RC component, as found for sample ST1300 (Fig. 5D), and the fitting parameters extracted from the Nyquist plots should thus correspond to:

$$C \approx C_B + C_{br} \tag{12}$$

$$R \sim R_{br} \tag{13}$$

Sample ST1400 possesses relatively low grain size (and thus low R_{agc}), and relatively low porosity, which corresponds to low R_{br}. In this case, the orders of magnitude of R_{agc} and R_{br} may be similar, as shown in Fig. 5C. The equivalent circuit shown in Fig. 10B was thus used to fit the impedance spectra of sample ST1400.

The orders of magnitude of capacitances also support the proposed mechanisms. According to the equivalent circuit proposed for dense samples their capacitance corresponds to the bulk capacitance [Eq. (10)]. The values obtained for samples ST1600 and ST1480 are thus within the same order of magnitude (Fig. 7), and the differences in $C_B = \varepsilon_o \varepsilon_r (A/L)_{ef}$ might be due to changes in the effective area to thickness ratio $(A/L)_{ef}$. The values of C_B obtained for sample ST1400 are also within the order of magnitude of the values obtained for samples ST1600 and ST1480. However, the capacitance of the bridging elements (C_{br}) is orders of magnitude greater than the bulk capacitance (Table 2) probably because the effective area to thickness ratio $(A/L)_{br}$ of these elements is much higher than in the bulk.

The bridging elements in the slightly porous samples are probably also related to the bulk properties. However, this still corresponds to a relatively small fraction of the contribution of grain interiors, and thus relatively small effective thickness to area ratio $(L/A)_{br}$. The resistance of the bridging element, $R_{br} = \rho_B (L/A)_{ef}$, is thus orders of magnitude smaller than the bulk resistance ($R_{br} << R_B$).

Vollman and co-authors[10] have already predicted channels with enhanced charge transport in reducing conditions, and ascribed this contribution to the onset of a Λ-type profile across grain boundaries. Although experimental evidence for this mechanism was not reported for bulk ceramic samples, differences in electrical behaviour observed for thick strontium titanate films with different grain sizes suggested microstructural contributions with enhanced charge transport along grain contacts.[16]

The resistances of all the samples converge at high temperatures, as expected for conditions when the overall resistance converges to the true bulk resistance. Nearly equilibrium conditions are more likely to occur in the high temperature range (700–1000 °C),[8,18] and these results were thus used to evaluate the activation energy (Fig. 6). The value obtained for sample ST1600 (2.38 eV) is probably the least affected by contributions other than the bulk, and may thus be compared to other results reported in the literature.[6,18] For example, on combining the values reported by Moos and Hardtl[6] for the enthalpy $\Delta H_R = 6.1$ eV of reaction

$$O_O^x \Longleftrightarrow VO^{\bullet\bullet} + 2e' + 1/2O_2. \tag{14}$$

and a slight temperature dependence of mobility,[6] $\mu_n = 614.\exp\{0.2\ \text{eV}/(\text{kT})\}\ \text{m}^2/(V.s)$, one should expect a typical activation energy $\Delta H_R/3 - E\mu_n = 1.83$ eV. This value is somewhat lower than our result. However, one may also expect higher temperature dependence of the concentration of charge carriers for cases when the concentration of oxygen vacancies tends to remain

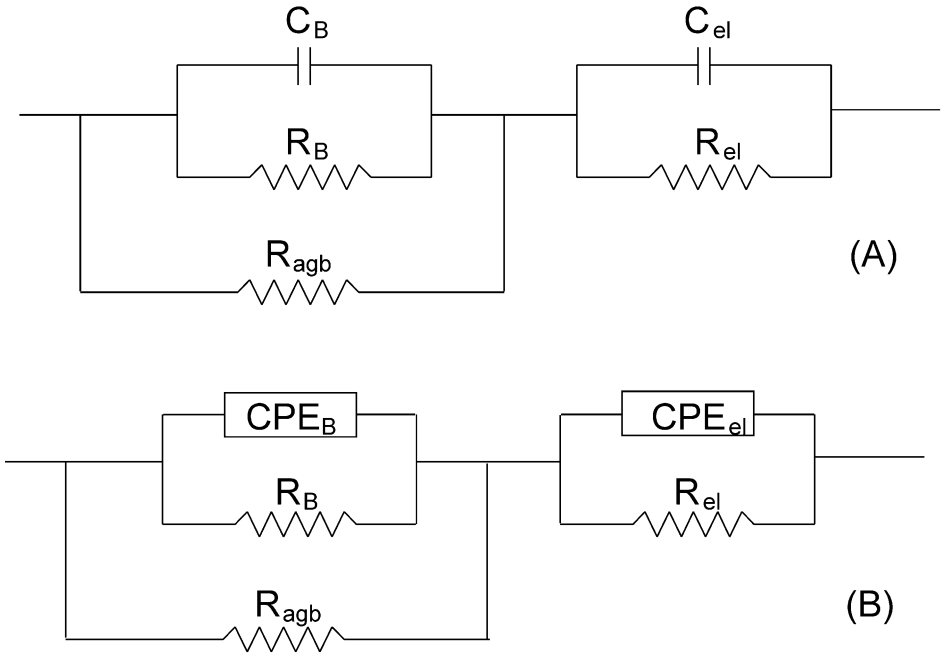

Fig. 9. Ideal equivalent circuit proposed for dense samples.

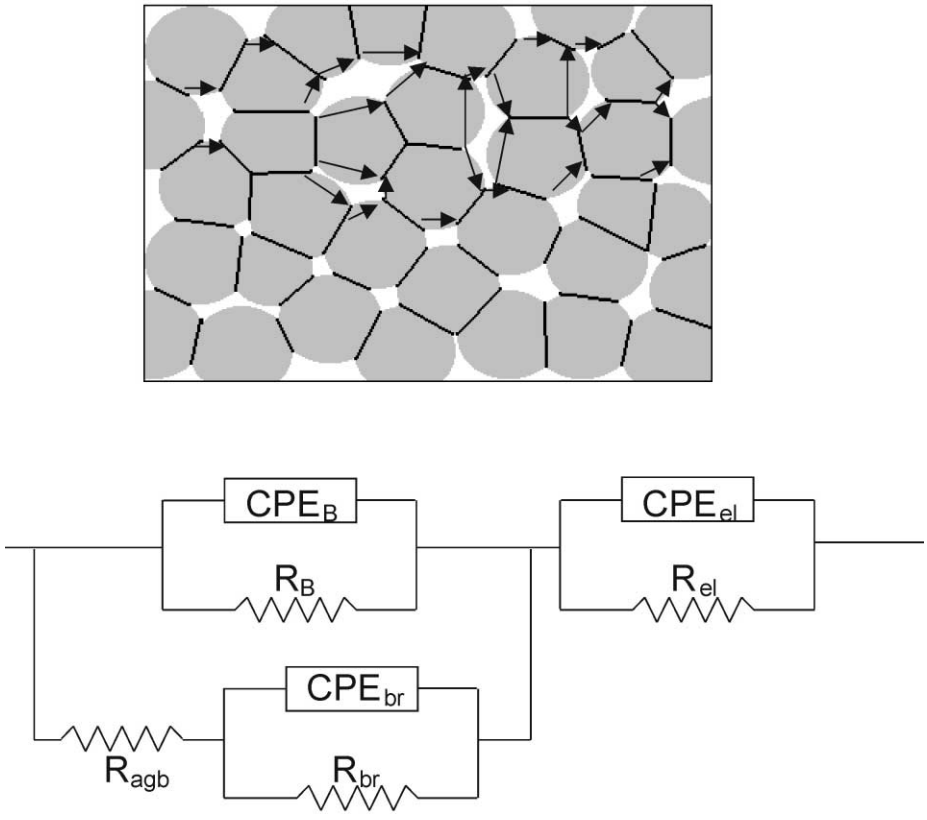

Fig. 10. Schematic representation of enhanced grain boundary transport in porous samples (A), and the proposed equivalent circuit.

nearly temperature independent, by becoming nearly frozen, or being controlled by impurities. In these cases the activation energy of conductivity should tend to $\Delta H_R/2 - E\mu_n = 2.85$ eV. In addition, there is some uncertainty about the correct value of ΔH_R, as reported by different authors.[6,18] The values of activation energy obtained from the conductivity results are thus inconclusive about the relevant defect chemistry even for the simplest cases when bulk contribution predominates, and nearly equilibrium conditions are more likely to occur.

Table 2
Values of dielectric constant extracted from capacitance obtained by fitting the impedance spectra of samples ST1600 and ST1400

ST1600		ST1400	
T (°C)	$C_B(L/A)/\varepsilon_o$	$C_B(L/A)/\varepsilon_o$	$C_{br}(L/A)/\varepsilon_o$
300	830	1112	2.84×10^4
325	805	1082	2.77×10^4
350	778	1020	2.71×10^4
375	756	964	2.69×10^4
400	719	903	2.76×10^4
425	701	903	3.20×10^4
450	682	903	3.85×10^4

5. Comments on the effects of reoxidation kinetics

The enthalpy of reaction 14 is relatively high, and one may predict decrease in the corresponding equilibrium constant on cooling, and thus oxygen uptake. For example, the value $\Delta H_R = 6.1$ eV[6] yields

$$\left[V_O^{\bullet\bullet}\right]n^2/P_{O_2}^{1/2} = \exp(\Delta S/R).\exp\left(-70.8\times10^3/T\right) \qquad (15)$$

and the equilibrium constant should decrease by a factor of about 2×10^{-16} on cooling from 1000 to 500 °C. However, equilibrium is unlikely to be retained at temperatures below about 700 °C, thus effecting the electrical properties at lower temperatures. One must thus play attention to the effects of cooling conditions on the kinetics of reoxidation. Actually, moderate changes in the cooling rates or gas flow rate do not exert significant effects on the relevant results, at least in the actual ranges of working conditions (Figs. 3 and 4).

One may also consider the role of grain boundaries on the kinetics of reoxidation. For example, formation of core-shell structures in some donor-doped titanate materials[19] may suggest that grain boundaries reoxidise faster than the grain interiors; this may explain major differences between the conductivity results reported for single crystals and ceramic samples of donor-doped strontium titanate.[20] However, the role of grain boundaries on the kinetics of reoxidation is still debatable because Wernicke[21] did not find significant differences between the reoxidation kinetics of dense titanate samples with small (2 μm) and large (100 μm) grain sizes. Note that faster reoxidation, and thus higher resistance should be expected for dense samples with smaller grain size. Our results (Fig. 6) show the opposite trend thus confirming that enhanced transport along grain contacts is a much more consistent explanation for the effects of grain size on the behaviour of strontium titanate ceramics in reducing conditions.

6. Conclusions

The overall resistance of dense strontium titanate ceramic samples increases markedly with increasing average grain size, thus reverting the trend observed in oxidizing conditions; this suggests enhanced charge transport along multiple grain contacts in parallel with charge transport in the bulk. Channels with enhanced charge transport might thus explain some differences between results obtained by different authors, except possibly at very high temperatures when the overall behavior still tends to be controlled by transport in the bulk. However, further work is needed to confirm the nature of those channels with enhanced charge transport.

The overall resistance of porous samples is much higher than expected for the corresponding grain size. However the resistance of dense samples with coarse grain size is still higher. These differences were interpreted on assuming that the channels with enhanced charge transport may be interrupted by pores, thus requiring a partial contribution of charge transport through the interior of grains.

Acknowledgements

This work was sponsored by the Portuguese Foundation for Science and Technology (FCT), and under Contract PRAXIS/3/3.1/MMA/1760/95.

References

1. Yamaoka, N. and Matsui, T., Properties of $SrTiO_3$-based boundary layer capacitors. In *Advances in Ceramics, Vol. I, Grain Boundary Phenomena in Electronic Ceramics*, ed. L. M. Levinson and D. C. Hill. American Ceramic Society, Columbus, OH, 1981, pp. 232–241.
2. Wernicke, R., Two layer model explaining the properties of $SrTiO_3$ boundary layer capacitors. In *Advances in Ceramics, Vol. I, Grain Boundary Phenomena in Electronic Ceramics*, ed. L. M. Levinson and D. C. Hill. American Ceramic Society, Columbus, OH, 1981, pp. 272–281.
3. Peng, C. J. and Chiang, Y. M., Grain growth in donor-doped $SrTiO_3$. *J. Mater. Res.*, 1990, **5**(6), 1237–1245.
4. Bae, C., Park, J. G., Kim, Y. H. and Jeon, H., Abnormal grain growth of niobium-doped strontium titanate ceramics. *J. Am. Ceram. Soc.*, 1998, **81**, 3005–3009.
5. Cho, S. G. and Johnson, P. F., Evolution of microstructures of undoped and Nb-doped $SrTiO_3$. *J. Mater. Sci.*, 1994, **29**, 4866–4874.
6. Moos, R. and Hardtl, K. H., Defect chemistry of donor-doped and undoped strontium titanate ceramics between 1000 °C and 1400 °C. *J. Am. Ceram. Soc.*, 1997, **80**, 2549–2562.
7. Abrantes, J. C. C., Labrincha, J. A. and Frade, J. R., Evaluation of $SrTi_{1-y}Nb_yO_{3+\delta}$ materials for gas sensors. *Sensors and Actuators B*, 1999, **19**, 773–776.
8. Chan, N. H., Sharma, R. K. and Smyth, D. M., Nonstoichiometry in $SrTiO_3$. *J. Electrochem. Soc.*, 1981, **128**, 1762–1769.
9. Vollman, M. and Waser, R., Grain boundary defect chemistry of acceptor-doped titanates: space charge layer width. *J. Am. Ceram. Soc.*, 1994, **77**, 235–243.

10. Vollman, M., Hagenbeck, R. and Waser, R., Grain boundary defect chemistry of acceptor-doped titanates: inversion layer and low field conduction. *J. Am. Ceram. Soc*., 1997, **80**, 2301–2314.
11. Denk, I., Claus, J. and Maier, J., Electrochemical investigations of $SrTiO_3$ boundaries. *J. Electrochem. Soc*., 1997, **144**, 3526–3536.
12. Bauerle, J. E., Study of solid electrolyte polarization by a complex admittance method. *J. Phys. Chem. Sol*., 1969, **30**, 2657–2670.
13. Fleig, J. and Maier, J., A finite element study on the grain boundary impedance of different microstructures. *J. Electrochem. Soc*., 1998, **145**, 1781–1789.
14. Abrantes, J. C. C., Labrincha, J. A. and Frade, J. R., Applicability of the brick layer model to describe the grain boundary properties of strontium titanate ceramics. *J. Eur. Ceram. Soc*., 2000, **20**, 603–609.
15. Hagenbeck, R. and Waser, R., Simulation of the charge transport across and along grain boundaries in titanate ceramics for the small signal regime. In *Electroceramics V, Vol. II*, ed. J. L. *et al* Baptista. Fundação João Jacinto Magalhães, Aveiro, Portugal, 1996.
16. Gerblinder, J., Hausner, M. and Meixner, H., Electric and kinetic properties of screen-printed strontium titanate films at high temperatures. *J. Am. Ceram. Soc*., 1995, **78**, 1451–1456.
17. Boukmap, B., A nonlinear least squares fit procedure for analysis of immitance data of electrochemical systems. *Solid State Ionics*, 1986, **20**, 31–44.
18. Choi, G. M. and Tuller, H. L., Defect structure and electrical properties of single crystal $Ba_{0.03}Sr_{0.97}TiO_3$. *J. Am. Ceram. Soc*., 1988, **71**, 201–205.
19. Chung, S. Y., Lee, B. K. and Kang, S. J. L., Core-shell structure formation in Nb_2O_5-doped $SrTiO_3$ by oxygen partial pressure change. *J. Am. Ceram. Soc*., 1998, **81**, 3016–3018.
20. Moos, R. and Hardtl, K. H., Electronic transport properties of $Sr_{1-x}La_xTiO_3$ ceramics. *J. Appl. Phys*., 1996, **80**, 393–400.
21. Wernicke, R., The kinetics of equilibrium restoration in barium titanate ceramics. *Philips Res. Repts*., 1976, **31**, 526–543.